



The scale size of chondrule formation regions: Constraints imposed by chondrule cooling rates

LON L. HOOD* AND FRED J. CIESLA

Lunar and Planetary Laboratory, University of Arizona, Tucson, Arizona 85721-0092, USA

*Correspondence author's e-mail address: lon@lpl.arizona.edu

(Received 2001 June 11; accepted in revised form 2001 September 10)

Abstract—Meteoritic data strongly suggest that most chondrules reached maximum temperatures in a range of 1650–2000 K and cooled at relatively slow rates of 100–1000 K/h, implying a persistence of external energy supply. The presence of fine-grained rims around chondrules in most unequilibrated chondrites also indicates that a significant quantity of micron-sized dust was present in chondrule formation regions. Here, we assume that the persistent external energy source needed to explain chondrule cooling rates consists primarily of radiation from surrounding heated chondrules, fine dust, and gas after the formation event. Using an approximate one-dimensional numerical model for the outward diffusion of thermal radiation from such a system, the scale sizes of formation regions required to yield acceptable cooling rates are determined for a range of possible chondrule, dust, and gas parameters. Results show that the inferred scale sizes depend sensitively on the number densities of micron-sized dust and on their adopted optical properties. In the absence of dust, scale sizes >1000 km are required for plausible maximum chondrule number densities and heated gas parameters. In the presence of dust with mass densities comparable to those of the chondrules and with absorptivities and emissivities of ~0.01 calculated for Mie spheres with a pure mineral composition, scale sizes as small as ~100 km are possible. If dust absorptivities and emissivities approach unity (as may occur for particles with more realistic shapes and compositions), then scale sizes as small as ~10 km are possible. Considering all uncertainties in model parameters, it is concluded that small scale sizes (10–100 km) for chondrule formation regions are allowed by the experimentally inferred cooling rates.

INTRODUCTION

It is important to understand the origin of chondrules because of their prevalence in primitive (chondritic) meteorites and because of the clues that they may therefore provide about the early accretional period of solar system formation. Most detailed analyses have inferred that these millimeter-sized, once-molten inclusions formed in short-duration heating events in a relatively cool, dust-rich solar nebula environment (Taylor *et al.*, 1983; Wood, 1984; Hewins, 1988; Grossman *et al.*, 1988; Grossman, 1988, 1996). Many chondrules have apparently been thermally processed repeatedly and some contain recycled fragments of previous generations of chondrules (Kring, 1988, 1991; Alexander, 1994). Multiple heating events are therefore indicated. Similar, but somewhat modified, characteristics have been inferred for larger calcium-aluminum-rich inclusions (CAIs) that are prevalent in some carbonaceous chondrites (MacPherson *et al.*, 1988).

In addition to the basic requirement of rapid, multiple heating events in a relatively cool nebula, meteoritic data have

imposed several additional constraints that must be satisfied by any successful chondrule formation model. Among these are the experimentally derived temperature conditions of chondrule formation. Results of dynamic crystallization experiments performed by Hewins and Radomsky (1990) and others suggest that some chondrule textures (*e.g.*, porphyritic, granular) formed with initial maximum temperatures below the liquidus while other textures (*e.g.*, glassy, non-porphyritic) formed after complete melting. A survey of chondrules in carbonaceous and ordinary chondrites showed that few chondrules with liquidus temperatures over 1750 °C were non-porphyritic (completely melted) (Hewins and Radomsky, 1990). On the other hand, few chondrules with liquidus temperatures below 1400 °C were porphyritic (incompletely melted). It was therefore inferred that most chondrules were heated to initial temperatures in the range of 1400–1750 °C (about 1650–2000 K). Furthermore, the common occurrence of barred olivine textures and porphyritic textures showing igneous zoning for iron, magnesium, and calcium in olivine crystals were consistent with cooling rates in the range of 100–1000 K/h. This cooling rate

is most applicable at temperatures below the liquidus and solidus (~ 1400 to 1800 K) and is much slower than that expected for free radiation to space ($\sim 10^6$ K/h), implying a persistence of external energy supply.

Currently, the mechanism(s) responsible for providing the necessary repetitive, short-duration heating events in a low-temperature (< 650 K) solar nebula have not been positively identified (for reviews, see Boss, 1996; Hewins, 1997). One leading candidate mechanism hypothesizes the occurrence of gas-dynamic shock waves in the nebula (Wood, 1984; Hood and Horanyi, 1991; Connolly and Love, 1998). It can be shown, for example, that shocks with Mach numbers greater than 4 or 5 would be capable of thermally processing and melting 0.1 – 1 mm sized precursor aggregates as required by meteoritic data (Wood, 1984; Hood and Horanyi, 1991, 1993). Near the nebula midplane, possible energy sources for generating multiple shocks include spiral density waves or mass concentrations in a gravitationally unstable nebula (Wood, 1996; Boss, 2000) and bow waves upstream of planetesimals scattered gravitationally into eccentric/inclined orbits by proto-Jupiter (Hood, 1998; Weidenschilling *et al.*, 1998). Other chondrule formation mechanisms that have been proposed include nebular lightning (*e.g.*, Desch and Cuzzi, 2000), collisional disruption of radiogenically heated planetesimals (Lugmair and Shukolyukov, 2001), and thermal processing in proto-stellar winds (Shu *et al.*, 2001).

A potentially important constraint on chondrule formation mechanisms is the scale size of chondrule formation events. For example, the gravitational instability shock wave mechanism predicts relatively large-scale sizes ($> 10\,000$ km) for shock-heated regions while the planetesimal bow wave and nebular lightning mechanisms predict smaller scale sizes (~ 10 km). If only large-scale sizes for chondrule formation regions are permitted by independent evidence, then the planetesimal bow wave and lightning mechanisms would be disfavored. Several recent numerical simulations of the shock wave heating model of chondrule formation have yielded acceptable cooling rates (Iida *et al.*, 2001; Desch and Connolly, 2001; Ciesla and Hood, 2001). In these models, the scale size of the chondrule formation region is very large ($> 10\,000$ km), optically thin, and the solids-to-gas mass ratio is near to that expected for condensation from a nebula of solar composition. Under such conditions, the chondrule cooling rate is determined by extended drag heating as the chondrule-gas velocity decreases in a low-density nebula (Iida *et al.*, 2001) and by the rate of energy loss from the shock-heated gas downstream from the shock. The latter is influenced by thermal radiation from solids so that the cooling rate actually increases with increasing dust density (Desch and Connolly, 2001; Ciesla and Hood, 2001). Since these models predict very large scale sizes for chondrule formation regions, they are most compatible with large-scale shock generation mechanisms (*e.g.*, the gravitational instability mechanism; Wood, 1996; Boss, 2000).

In this paper, we consider an alternate case in which chondrule formation regions are optically thick and are

characterized by higher solids-to-gas mass ratios than expected for condensation from a solar composition nebula. In this case and for sufficiently large concentrations of particles, the cooling rate decreases with increasing particle number densities. Meteoritic evidence suggesting that relatively high solids-to-gas ratios in chondrule formation regions are possible or likely is reviewed in "Meteoritic Constraints on the Chondrule Formation Environment" below. Other evidence indicating relatively high gas pressures and densities, probably resulting from partial vaporization of preexisting silicates, is also reviewed. Finally, recent interpretations of chondrule fine-grained rims as being a consequence of the hypersonic interaction of freshly formed chondrules with a mixture of gas and small-scale dust is reviewed. The latter interpretations are consistent with the presence of significant quantities of fine dust in chondrule cooling regions. On the basis of this evidence, we then investigate the scale size of chondrule formation regions under the assumption that the persistent energy supply responsible for chondrule cooling rates is provided by radiation from surrounding heated chondrules, micron-sized dust, and gas.

The investigation is not applicable only to the shock model since other chondrule formation models (*e.g.*, nebular lightning) could also result in formation regions that would cool radiatively. However, in the context of the shock model, such a situation may arise if a nebular shock wave encounters a zone that is enriched in chondrule-sized particles and micron-sized dust (Fig. 1). After passage of the shock, a region of melted chondrules, partially vaporized or condensing dust, and heated gas would remain that would cool radiatively at a rate determined mainly by its own size and opacity.

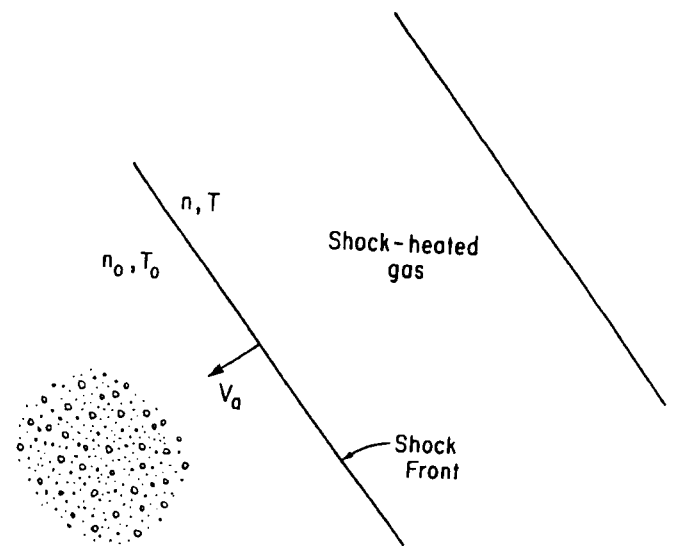


FIG. 1. Schematic illustration of the nebular shock wave model for the special case in which a concentration of precursor particles and fine dust encounters a gas dynamic shock. The diagonal lines indicate that the region of shock-heated gas is finite in extent because of post-shock cooling processes.

For the purpose of a quantitative analysis, an approximate model for the outward diffusion of thermal radiation from a one-dimensional slab containing chondrules, fine dust, and heated gas is formulated in "Model Formulation". Results of numerical simulations for a series of possible chondrule and dust number densities and optical parameters are given in "Model Results". Implications of the results for chondrule formation models such as the shock wave model are discussed in "Discussion and Implications".

Sahagian and Hewins (1992) previously investigated a closely related problem by calculating the loss of thermal radiation from a uniformly heated infinite slab whose opacity was controlled by the concentration of both chondrules and micron-sized dust. However, their model was not explained in detail and values for several key parameters (*e.g.*, particle emissivities) were not explicitly given. Adopting a number density for chondrules of $\sim 10 \text{ m}^{-3}$, they found that $\sim 80\%$ of a 1000 km thick slab had a cooling rate in the 100–1000 K/h range. By adding a dispersion of micron-sized dust representing $0.135\times$ the mass of the chondrules, it was found that smaller slab thicknesses of ~ 100 km would yield acceptable cooling rates throughout most of the slab. From these results, they concluded that the concentration of micron-sized dust was the key to determining whether chondrules formed in large-scale events or in small, localized events. Here, we employ an independent model to investigate more completely the minimum scale size of chondrule formation regions allowed for a series of possible solids-to-gas mass ratios, heated gas densities, and mass fractions of micron-sized dust.

METEORITIC CONSTRAINTS ON THE CHONDRULE FORMATION ENVIRONMENT

In support of the model to be developed in "Model Formulation", we review briefly here meteoritic evidence relating to the environmental conditions within chondrule formation regions. Meteoritic evidence relating to solids concentrations, gas composition, and gas pressure in chondrule formation regions is specifically examined.

Solid Particle Densities and Gas Oxygen Fugacities

The term "solids" is defined here as silicate-rich material containing all elements but H and noble gases. Solids can therefore include both millimeter-sized chondrules and small-scale "dust". Volatile-rich material (*i.e.*, solids of cometary composition) are assumed to be absent or negligible in concentration in the chondrule formation region. The solids-to-gas atomic ratio is most often employed by cosmochemists and is defined as the atomic Si/H ratio divided by the solar Si/H ratio. However, for our purposes in this paper, it is convenient also to consider the solids-to-gas mass ratio, which has a value of ~ 0.005 for a parcel of material of solar bulk composition at ~ 400 K (*e.g.*, Krot *et al.*, 2001).

Gooding and Keil (1981) used measurements of compound and cratered chondrules together with upper limits on chondrule relative velocities to estimate the number densities of chondrules during the period when they were in a partially molten or "plastic" state. For the most common (incompletely melted, porphyritic) chondrules, number densities in the range of $1\text{--}100 \text{ m}^{-3}$ were estimated. Here, we reexamine this estimate in view of more recent data on chondrule thermal histories and relative velocities.

Following Gooding and Keil, the chondrule number density N may be estimated using an approximate model for colliding molecules as derived from the kinetic molecular theory of gases (*e.g.*, Barrow, 1966),

$$N = P / (2^{1/2} \pi d^2 \bar{v} \bar{t}) \quad (1)$$

where P is the measured collision probability, d is the chondrule diameter (assuming identical, spherical chondrules), \bar{v} is the average speed of each chondrule, and \bar{t} is the average time spent by a chondrule in a deformable or "plastic" state. Based on the observed abundances of compound and cratered chondrules in a sample of >1600 specimens, Gooding and Keil estimated that the chondrule population value for P is in the range of 2 to 14%. An upper limit for \bar{v} of $\sim 10^4 \text{ cm s}^{-1}$ was estimated from the results of collision experiments indicating that higher velocities would have disrupted chondrules on impact. The fact that fragmented relic chondrules are present in chondrites implies that relative velocities did, at least occasionally, reach this upper limit. Finally, their experimentally inferred range for \bar{t} was "tens or hundreds of seconds or longer". Using these values, Eq. (1) yields $N > 0.5\text{--}3 \text{ m}^{-3}$.

However, actual *mean* relative velocities may have been less than the 10^4 cm s^{-1} upper limit assumed by Gooding and Keil. For example, Kring (1991) estimated relative velocities for molten droplets that coalesced with chondrules after their formation as $\leq 1.3 \text{ m/s}$. Also, 100 cm/s has been suggested as a typical velocity to prevent collisional destruction by Weidenschilling (1988). If we assume $\bar{v} \approx 1 \text{ m/s}$, then $N \approx 50\text{--}300 \text{ m}^{-3}$. On the other hand, as noted in the Introduction, experimental simulations suggest that chondrule cooling rates near solidus temperatures were in the range of 100–1000 K/h (Hewins and Radomsky, 1990). If chondrules remained in a deformable state over a temperature interval of order 100 K, then the actual mean time spent by most chondrules in this state may have been 0.1–1 h, or $\sim 10^3 \text{ s}$. Experimental simulations also suggest that 10^3 s is a reasonable timescale for plasticity (Radomsky and Hewins, 1990). For this value of \bar{t} , we have $N \approx 5\text{--}30 \text{ m}^{-3}$. For comparison, a similar evaluation of experimental results by Sahagian and Hewins (1992) yielded an estimated chondrule number density of 10 m^{-3} . Considering all uncertainties, the original range estimated by Gooding and Keil (1981) of about $1\text{--}100 \text{ m}^{-3}$ still seems appropriate.

An alternate constraint on the solids-to-gas mass ratio and chondrule number density is the unexpectedly large fayalite

content of olivine in chondrules, implying that O/H in the nearby nebula may have been ~ 100 to $\sim 1000\times$ the solar value (Wood, 1985). While a few recent studies indicate that some chondrules may have experienced equilibration with a gas of nearly solar composition (Beckett and Stolper, 2001), other studies are consistent with the hypothesis that most chondrules formed in an oxygen-rich environment, implying that substantial quantities of (partially vaporized) silicate solids were present (Wood, 1985). The required solids enrichment is of the same order as the O/H enrichment. Consistent with this estimate, Lauretta *et al.* (2001) have recently inferred solids/gas atomic ratios of about $300\text{--}350\times$ the solar value from studies of metals derived from chondrule melts in the Bishunpur ordinary chondrite. Finally, Ebel and Grossman (2000) assume solids enrichments between 600 and $1000\times$ that expected to have condensed from a gas of solar composition in order to explain both the FeO contents of silicates and the compositions of glasses in chondrules. Such an enrichment implies a solids-to-gas mass ratio of at least 3 to 5.

On the other hand, the analyses of Wood (1985), Ebel and Grossman (2000), and Lauretta *et al.* (2001) assumed thermodynamic equilibrium during chondrule formation. It is possible (or even likely) that chondrule formation was not an equilibrium process but that the process was more stochastic and the precursors were heterogeneous (*e.g.*, Sears *et al.*, 1996). Thus, the direct interpretation of chondrule compositions in terms of nebula composition and solids-to-gas mass ratios may not be as straightforward as assumed above.

Gas Pressures and Densities in Formation Regions

Based on magnesium isotope measurements of whole chondrules from the Allende meteorite, Galy *et al.* (2000) have recently emphasized that relatively high gas pressures must have prevailed in the chondrule formation region. Specifically, they infer pressures exceeding 1 hPa (10^3 dynes cm^{-2}) in order to explain high evaporation rates implied by correlations between measured Mg isotope ratios, Mg/Al ratios, and chondrule sizes. Similarly, Ebel and Grossman (2000) have found that chondrule glass compositions are explained by either high solids enrichment or high total gas pressures (~ 1 hPa), or both. For comparison, a typical gas number density for a low-mass nebula in the asteroid belt region is 2×10^{14} cm^{-3} (Appendix A). At a nominal temperature of 400 K, the corresponding gas pressure is ~ 0.01 hPa. Thus, the inferred gas pressures in chondrule formation regions are at least several orders of magnitude higher than expected for the midplane of a quiescent, low-mass nebula at radial distances where chondrules are likely to have formed.

It is unlikely that the inferred high gas pressures can be explained by shock processing of nebular gas alone. For example, an adiabatic Mach 5 shock in the nominal nebula considered above (number density 2×10^{14} cm^{-3} ; temperature 400 K) produces a post-shock gas pressure of 0.4 hPa. The high inferred gas pressures (>1 hPa) together with the high

inferred oxygen fugacities are most plausibly explained by partial vaporization of more volatile chondrule constituents during the chondrule formation process. Adopting the shock wave model, this implies that partial vaporization occurred during passage of the shock front.

If gas pressures were indeed high in chondrule formation regions and if the gas contained a significant component of silicate vapor, then it follows that gas mass densities were also relatively high. For example, a gas pressure of 1 hPa at a temperature of ~ 1500 K implies a number density of $n_g = 4.8 \times 10^{15}$ cm^{-3} . In order to estimate the mean molecular mass of nebular gas mass-loaded with silicate vapor, we consider a system of H, He, O, C, S, Si, Mg, Fe, Al, Ca, and Na, where H, He, and C are found originally in only the gas phase, O is in both the gas and solid phases, and the rest are condensed in dust (following Wood and Hashimoto, 1993). The latter authors give the cosmic abundance of each element and the abundance in the dust phase (abundances are given in number of atoms relative to Si). Let the dust concentration factor F be that relative to the dust concentration expected for condensation from a gas of solar composition. Then the number density of a given element is obtained by multiplying F times the abundance in the dust phase and adding the result to the abundance in the gas phase. Assuming that the gaseous species are atomic He, Fe, Na, Ca, Al, Mg, and molecular SiO, CO, H₂S, H₂O, and H₂, it is then straightforward to calculate the mean molecular mass. Assuming total vaporization of the dust, the mean molecular mass of the gas mixture for $F = 1$ is 4.72×10^{-24} g. For $F = 10$, it is 4.91×10^{-24} g; for $F = 100$, it is 6.76×10^{-24} g; for $F = 1000$, it is 21.9×10^{-24} g. As discussed in the previous subsection, solids enrichments in the range of ~ 100 to $1000\times$ solar are possible in chondrule formation regions. Thus, the mean molecular mass may have ranged from ~ 6 to 22×10^{-24} g. Since the above calculation neglected H₂ dissociation, the lower end of this range may be more appropriate. Therefore, conservatively taking the mean mass to be $\sim 6 \times 10^{-24}$ g, the gas mass density corresponding to a gas pressure of 1 hPa and a temperature of 1500 K is $\sim 3 \times 10^{-8}$ g cm^{-3} .

Evidence for a Small-Scale Dust Component

Fine-grained rims (dust mantles) are present around chondrules in most unequilibrated chondrites and have characteristics suggesting formation within the solar nebula (Metzler *et al.*, 1992; Metzler and Bischoff, 1996). Connolly and Love (1998) proposed that these rims were a consequence of hypersonic/supersonic interaction of a mixture of gas and small-scale (microns to tens of microns in size) dust with freshly formed chondrules in nebular shock waves. Numerical simulations by Liffman and Toscano (2000) demonstrate that their proposal is plausible for dust-to-gas mass ratios of about 0.5–1.0, provided that dust-chondrule sticking coefficients were in the range of 0.5–1.0. Smaller sticking coefficients would require larger dust-to-gas mass ratios.

In this regard, it is of interest to compare the thermal and dynamical histories of single micron-sized and millimeter-sized solids encountering nebular shocks. The numerical method for integrating the equations of gas-particle energy and momentum transfer has been described in Hood and Horanyi (1991, 1993). Figure 2 shows the history of an 0.5 mm radius forsterite particle after passage of an adiabatic Mach 4.3 shock in a nebula with initial number density $2.5 \times 10^{14} \text{ cm}^{-3}$ and an initial temperature of 400 K. For this particle composition, the emissivity was assumed to be ~ 0.8 . Figure 3 shows the history of an $0.5 \mu\text{m}$ radius forsterite particle (assumed emissivity, 2×10^{-3} ; see Fig. 2a of Rizk *et al.*, 1991) after passage through the same Mach 4.3 shock. (For a discussion of uncertainties in dust emissivities and absorptivities, see "Model Formulation".) The millimeter-sized particle (Fig. 2) is partially melted within 6 s and traverses a distance of $\sim 55 \text{ km}$ in 11 s while decelerating to a speed of 4.3 km/s relative to the shocked gas. Although only the first 11 s of the particle history is shown, the particle continues to decelerate with time until its speed relative to the shocked gas

approaches zero. In contrast, as shown in Fig. 3, the micron-sized particle traverses a distance of only 0.12 km in 0.028 s while decelerating to a relative speed of 2.7 km/s. As expected, this particle is therefore decelerated much more rapidly than the millimeter-sized particle. About 40% of the micron-sized particle is vaporized in this example. A comparison of the second panels of Figs. 2 and 3 therefore shows that there is a relative velocity of several kilometers per second between small-scale and chondrule-sized particles. As discussed further in "Discussion and Implications" below, this relative velocity may have been an essential component of the process that led to rim formation.

Solid Particle Concentration Mechanisms

The inferred chondrule number densities and solids-to-gas mass ratios discussed above imply a concentration of solid particles in the nebula by a factor of as much as 1000 \times relative to that expected *via* condensation from a nebula of solar composition. One plausible mechanism for concentrating chondrule-sized particles in the nebula is differential transport in turbulent eddies (Cuzzi *et al.*, 1996, 2001). Cuzzi *et al.* (1996) found that under typical inner nebula conditions, particles with the size and density of chondrules would be

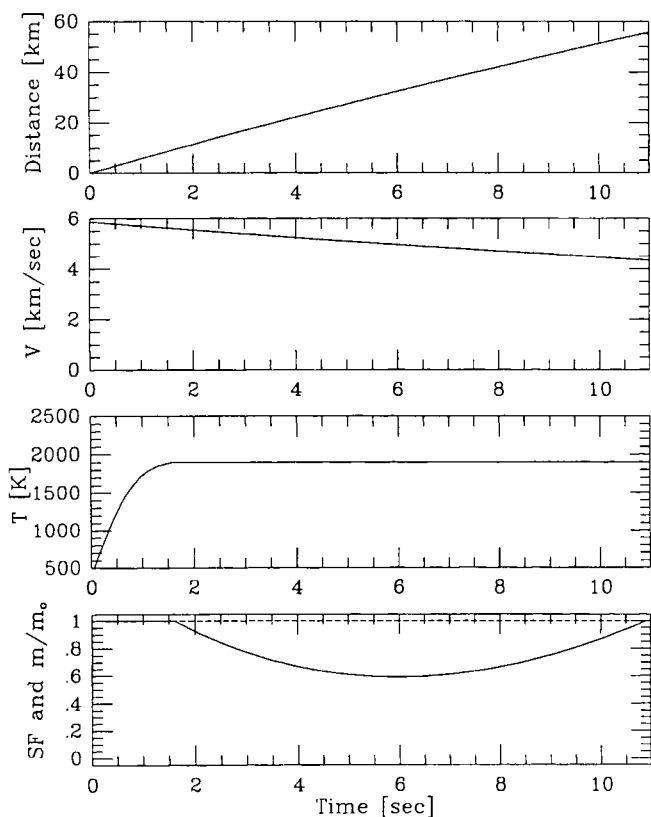


FIG. 2. One-dimensional dynamical and thermal history of an 0.1 mm radius forsterite particle after passage of an adiabatic Mach 5.2 shock. The pre-shock nebula number density and temperature were $2.5 \times 10^{14} \text{ cm}^{-3}$ and 400 K, respectively. The top panel shows the upstream distance traversed by the particle in the shocked gas. The second and third panels show the particle velocity relative to the gas and the particle temperature. The fourth panel shows the particle solid fraction (SF; solid line) and fractional mass (dashed line).

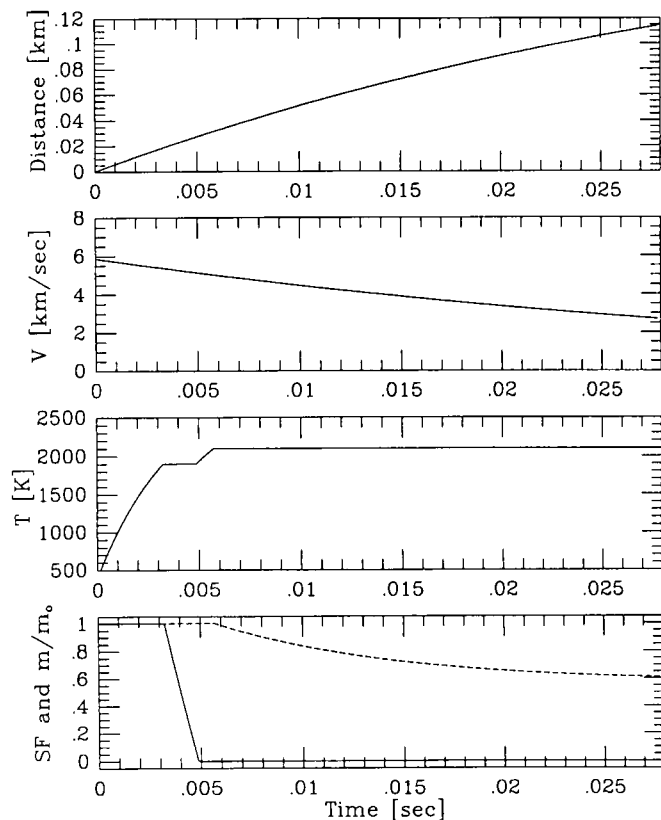


FIG. 3. Same format as Fig. 2 but for the case of an $0.5 \mu\text{m}$ radius forsterite particle. Note the scale change on the abscissa.

preferentially concentrated by turbulent transport. Concentration factors in dense zones reached 40–300 while, in extremely dense clumps, larger concentration factors of $>10^5$ were calculated (Cuzzi *et al.*, 2001). According to the model results, turbulent transport does not effectively concentrate fine dust, only chondrule-sized particles.

In addition to turbulent concentration, several other mechanisms for locally increasing the concentration of chondrules and/or fine dust can be suggested. First, collisions between planetesimals and high-velocity impacts on planetesimals may have resulted in enhanced solids concentrations. This mechanism may have been especially effective near resonances where swarms of planetesimals were accelerated gravitationally by proto-Jupiter (Weidenschilling *et al.*, 1998). Second, it is possible that nebular shocks themselves may have tended to effectively "sweep" particles into more concentrated zones before being processed by other shocks (see, for example, Hood and Horanyi, 1993).

MODEL FORMULATION

Given the evidence reviewed above that chondrules formed in regions where particle number densities, gas pressures and densities, and fine dust concentrations were significantly enhanced, we wish to investigate a model in which chondrule cooling rates are determined primarily by energy transfer from surrounding chondrules, gas, and dust. For this purpose, we consider in this section the problem of radiative cooling from a one-dimensional slab of chondrules, heated gas, and micron-sized dust. As indicated in the Introduction, this problem is not limited to the shock model but should be relevant for other formation models that consider chondrule formation in a solids-rich zone. The purpose of the model is to allow a quantitative investigation of the scale sizes of chondrule and dust concentrations that could yield acceptable cooling rates for a reasonable range of chondrule, dust, and gas parameters. The inferred scale sizes are of interest for distinguishing among possible mechanisms for generating shocks in the nebula, for example.

Consider an infinite slab of solid particles and gas as indicated schematically in Fig. 4. In general, both millimeter-sized chondrules and fine dust are present in the slab. In the context of the shock wave chondrule formation model, the situation envisaged here is a time immediately after passage of a shock through a solids-rich zone when all melted particles have re-solidified and are cooling radiatively and when vaporized silicates have begun to recondense (see, for example, Fig. 4 of Hood and Horanyi, 1993). The interspersed gas may consist of both shock-heated gas and silicate vapor. Radiation from the gas and any residual drag heating are neglected. However, the heat capacity of the gas is included since gas-dust energy transfer can occur by collisions of thermally driven gas molecules with solid particles. The initial temperature is T_0 . At $t = 0$ and at later times, all particles and gas are assumed

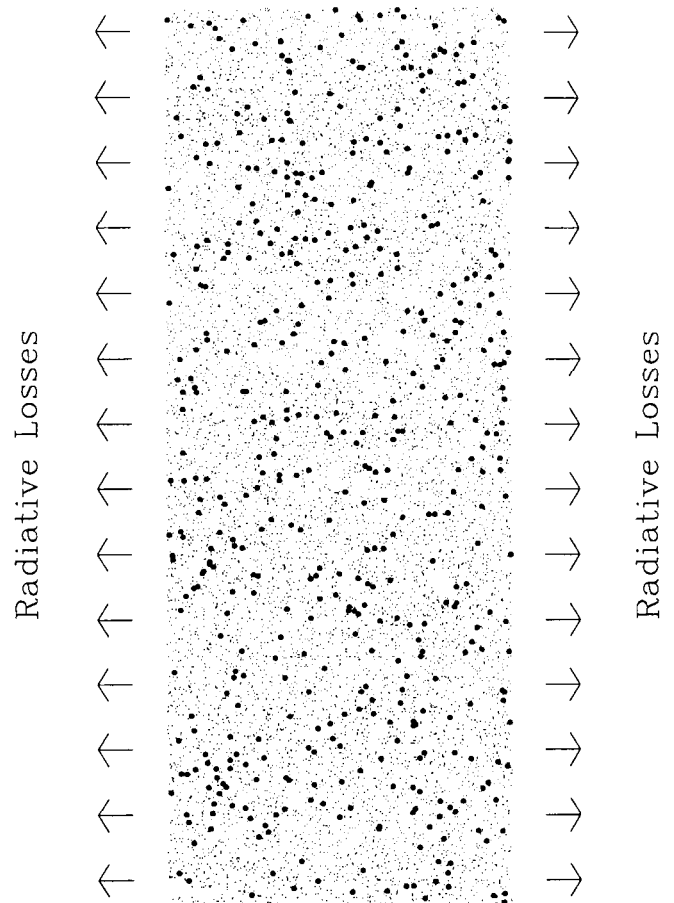


FIG. 4. Schematic illustration of an infinite slab of silicate particles and gas with the former consisting of both chondrule-sized precursors and micron-sized dust. All particles and gas are assumed to be at a common temperature T_0 at $t = 0$ and cool *via* the diffusion of thermal radiation from the slab.

to be at a common temperature and the system is assumed to cool solely by the outward diffusion of thermal radiation from the solid particles. Additional heating of the particles due to radiation from outside the slab is also neglected. The latter assumption may lead to an overestimate of actual chondrule cooling rates since some radiation from the receding shock front and/or from the protosun is expected.

The approximate numerical procedure for calculating the temperature profile in a slab containing only a monodispersion of identical spherical particles and gas as a function of time is described below. The modification of this procedure required for a particulate slab containing two size components (*e.g.*, millimeter-sized particles and micron-sized particles) is described in Appendix B.

First, the slab of width d is divided into a large number of parallel layers with thicknesses dx sufficiently small that mutual shadowing of particles in the layer is negligible. In that case, and neglecting radiation from the gas relative to that from the particles, the energy flux in the positive x direction out of the i th layer is given by (see Appendix C):

$$f_p(i) = \varepsilon_{em} n_p \sigma_p \sigma T_i^4 dx \quad (2)$$

where ε_{em} is the particle emissivity, n_p is the particle number density, σ_p is the particle cross section, σ is the Stefan–Boltzmann constant, and T_i is the (assumed constant) temperature within the layer. The energy flux in the negative x direction out of the same layer is $f_n(i) = -f_p(i)$. As shown in Appendix C, at a given boundary between layers, the perpendicular energy flux across the boundary is attenuated due to absorption in an adjacent layer by a factor of approximately $(1 - \varepsilon_{abs} n_p \sigma_p dx)$, where the condition $\varepsilon_{abs} n_p \sigma_p dx \ll 1$ is assumed to be valid.

If the total number of layers in the slab is N , there are $N + 1$ boundaries between layers. At the j th boundary, the energy flux across the boundary due to radiation from the i th layer is approximately

$$F(i, j) = f_p(i) \times (1 - \varepsilon_{abs} n_p \sigma_p dx)^n \quad (3)$$

for $j > i$ and

$$F(i, j) = f_n(i) \times (1 - \varepsilon_{abs} n_p \sigma_p dx)^n \quad (4)$$

for $j \leq i$, where ε_{abs} is the particle absorption coefficient and $n = |j - i - 1|$ for $j > i$ and $n = |j - i|$ for $j \leq i$. The total positively directed flux at the j th boundary due to radiation from all layers is

$$F_p(j) = \sum_{i=1}^{j-1} F(i, j) \quad (5)$$

and the total negatively directed flux at the j th boundary is

$$F_n(j) = \sum_{i=j}^N F(i, j) \quad (6)$$

Initially, at $t = 0$, the total thermal energy per unit area in the i th layer is $E_i = n_p m_p C_p T_i dx + \rho_g C_p^g T_i dx$, where m_p is the mass of a single solid particle, C_p is the specific heat of the particle, ρ_g is the gas mass density, and C_p^g is the gas specific heat. After a time increment dt , each layer gains an increment of energy of approximately

$$dE_g(i) = (F_p(j) + |F_n(j+1)|) dt \times (\varepsilon_{abs} n_p \sigma_p dx) \quad (7)$$

Simultaneously, the same layer loses a thermal energy increment of

$$dE_l(i) = (f_p(i) + |f_n(i)|) dt \quad (8)$$

At each time step, the total energy of each layer is adjusted according to $E_i(t + dt) = E_i(t) + dE_g(i) - dE_l(i)$. The temperature in each layer is then given by $T_i(t + dt) = E_i(t + dt) / (n_p m_p C_p dx + \rho_g C_p^g dx)$.

As a check of the validity of Eqs. (2) to (8), one may consider a limit in which the slab is infinitely thick and all layers are at the same temperature T . In that case, no cooling of the slab should occur and we should find that the energy gained by a layer in a given time increment Eq. (7) equals the energy lost Eq. (8). To verify that this is true, Eq. (5) can first be rewritten for a central layer as

$$F_p(j) = (\varepsilon_{em} n_p \sigma_p \sigma T^4 dx) \sum_{m=0}^{\infty} (1 - \varepsilon_{abs} n_p \sigma_p dx)^m \quad (9)$$

where j indicates the first (lowest x value) layer boundary and where a new summation index has been defined as $m = j - i - 1$. Eq. (9) becomes

$$F_p(j) = (\varepsilon_{em} / \varepsilon_{abs}) \sigma T^4 \quad (10)$$

where we have used the identity

$$\sum_{m=0}^{\infty} (1 - x)^m = 1/x$$

Similarly,

$$F_n(j+1) = -(\varepsilon_{em} / \varepsilon_{abs}) \sigma T^4 \quad (11)$$

Substituting Eqs. (10) and (11) into Eq. (7), one obtains

$$dE_g = (2\varepsilon_{em} n_p \sigma_p \sigma T^4 dx) dt \quad (12)$$

Evaluating Eq. (8) for the same layer gives

$$dE_l = (2\varepsilon_{em} n_p \sigma_p \sigma T^4 dx) dt \quad (13)$$

To carry out a given calculation, it is first necessary to choose a layer thickness dx and a time step dt . The layer thickness is chosen such that the condition $\varepsilon_{em} n_p \sigma_p dx \ll 1$ is satisfied. For the runs reported below, values of dx ranging from $d/100$ to $d/500$ were used. Time steps ranged from 0.1 to 0.001 s and were chosen such that the condition $dE_g(i) \ll E_i(t)$ and $dE_l(i) \ll E_i(t)$ is satisfied for all layers during the time integration.

Among the most important parameters in the above model are the particle emissivities and absorptivities. For the case of silicate particles with diameters near 1 μm , emissivities and absorptivities are near unity (we adopt a value of 0.8). However, the values of these optical constants for fine dust (e.g., micron-sized particles) are more difficult to estimate. For the case of perfectly spherical particles with a pure mineral (e.g., forsterite) composition, Mie theory may be applied to calculate emissivities as a function of wavelength (Rizk *et al.*, 1991). At temperatures of 1000–2000 K, peak emission wavelengths are in the range of 1 to 3 μm . At these wavelengths, pure forsterite spheres with radii of 1 μm would have emissivities near 2×10^{-3} while fayalite particles would have emissivities near $\sim 8 \times 10^{-2}$

(see Fig. 2 of Rizk *et al.*, 1991). For dominantly olivine dust particles containing both forsterite and fayalite, one might therefore estimate a mean emissivity of $\sim 10^{-2}$. In accordance with Kirchoff's law, the mean absorptivity would also be $\sim 10^{-2}$. On the other hand, actual fine dust particles in the solar nebula may have had a highly irregular shape (*e.g.*, fairy castle structures expected for accreted condensates) and may have contained a wide variety of mineral impurities. Such particles may have been more effective absorbers and emitters than Mie spheres with a purely monomineralic composition. Consequently, in the calculations to be presented below, a range of emissivities and absorptivities from 0.01 to 0.8 will be considered for micron-sized dust.

MODEL RESULTS

Figure 5 shows temperature profiles calculated using the above procedure for a slab of width 10 000 km containing only a monodispersion of particles with radii $\alpha = 0.5$ mm and no interspersed gas. For this calculation, the assumed particle properties were: number density, $n_p = 10 \text{ m}^{-3}$; mass density, $\rho_p = 2.5 \text{ gm cm}^{-3}$; emissivity, $\epsilon_{\text{em}} = 0.8$; absorptivity, $\epsilon_{\text{abs}} = 0.8$; cross section, $\sigma_p = \pi a^2$; specific heat, $C_p = 10^7 \text{ erg g}^{-1} \text{ K}^{-1}$; and

initial temperature, $T_0 = 1800 \text{ K}$. The total particle mass density is $\approx 1.3 \times 10^{-8} \text{ g cm}^{-3}$. As can be seen in the figure, most particles in the slab require nearly an hour to cool from 1800 to 1000 K. The cooling rate is therefore close to the experimentally inferred 100–1000 K/h range. As noted in the Introduction, experimentally inferred chondrule cooling rates are most applicable at temperatures below the liquidus and solidus (approximately 1400 to 1800 K). Cooling rates in Fig. 5 at these temperatures are somewhat higher than 1000 K/h. However, for the purpose of the present first-order analysis, mean cooling rates are estimated here in the 1000 to 1800 K temperature range. We note that this slab width (10 000 km) is an order of magnitude larger than that used by Sahagian and Hewins (1992) to obtain acceptable cooling rates for the same chondrule number densities. However, the agreement between our model results and theirs improves when fine dust is added (see below).

A repeat of the calculation of Fig. 5 using $n_p = 100 \text{ m}^{-3}$ (the upper limit of the allowed range estimated in "Solid Particle Densities and Gas Oxygen Fugacities") yields nearly identical cooling rates if the slab width is reduced to 1000 km (not shown here). The similarity between the cooling curves for these two cases follows from the sensitivity of the thermal diffusion rate to the optical depth of the slab, which is proportional to the product of the particle number density and the width. When micron-sized dust and interspersed gas are added (see below), the behavior is less predictable.

Figure 6 shows temperature profiles for the same case considered in Fig. 5 ($n_p = 10 \text{ m}^{-3}$; $T_0 = 1800 \text{ K}$) but with the addition of interspersed gas. The assumed gas properties are approximately appropriate for shocked nebular gas and vaporized dust ("Gas Pressure and Densities in Formation Regions"). Specifically, it is assumed that the gas number density is $5 \times 10^{15} \text{ cm}^{-3}$, that the mean molecular mass is $6 \times 10^{-24} \text{ g}$ (corresponding to vaporization of solids representing $\sim 100\times$ that expected for a gas of solar composition), and that the gas specific heat is approximately equal to that of molecular hydrogen, $C_p^g = 1.45 \times 10^8 \text{ erg K}^{-1} \text{ g}^{-1}$. The gas mass density ($3 \times 10^{-8} \text{ g cm}^{-3}$) corresponds to a pressure of 1 hPa at 1500 K ("Gas Pressure and Densities in Formation Regions") and is a factor of ~ 2 larger than the particle mass density given above. The width of the slab (2000 km) was purposely chosen to yield cooling rates comparable to those of Fig. 5. It is seen that the addition of the hot gas allows a smaller slab width (by a factor of 5) than was the case without including the gas heat capacity.

Figure 7 shows results for the same case considered in Fig. 6 except that the number density of chondrule-sized particles has been increased to 100 m^{-3} . Again, the width of the slab (600 km) was chosen to yield cooling rates comparable to those of Fig. 5. The increased chondrule number density reduces the outward diffusion of thermal radiation enough so that the necessary slab width is reduced by a factor of more than 3.

Since the upper bound on chondrule number densities ("Solid Particle Densities and Gas Oxygen Fugacities") is $\sim 100 \text{ m}^{-3}$, a solid particle radiation model can yield acceptable

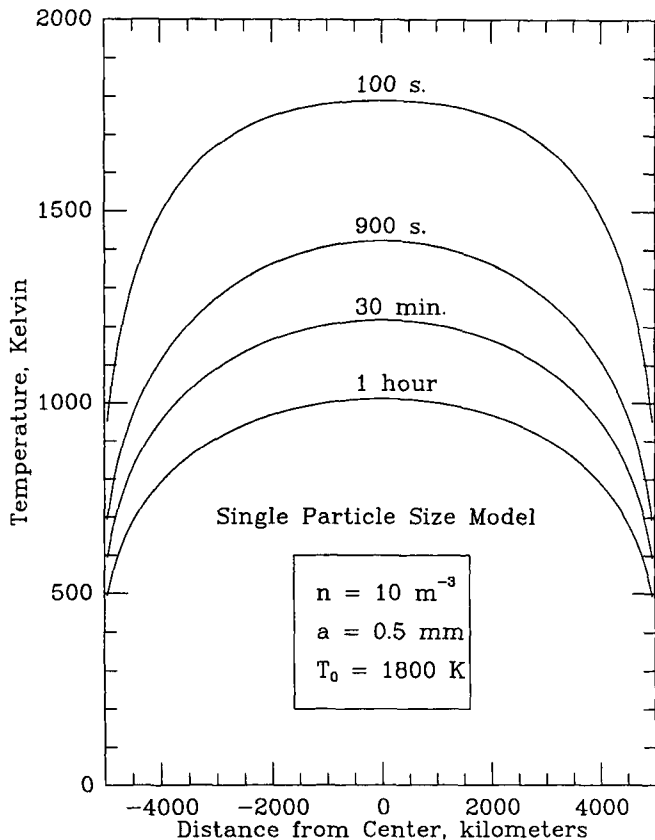


FIG. 5. Temperature profiles at selected times through a slab of width 10 000 km containing identical spherical particles with radii $\alpha = 0.5$ mm and with number density 10 m^{-3} . See the text for other model parameters.

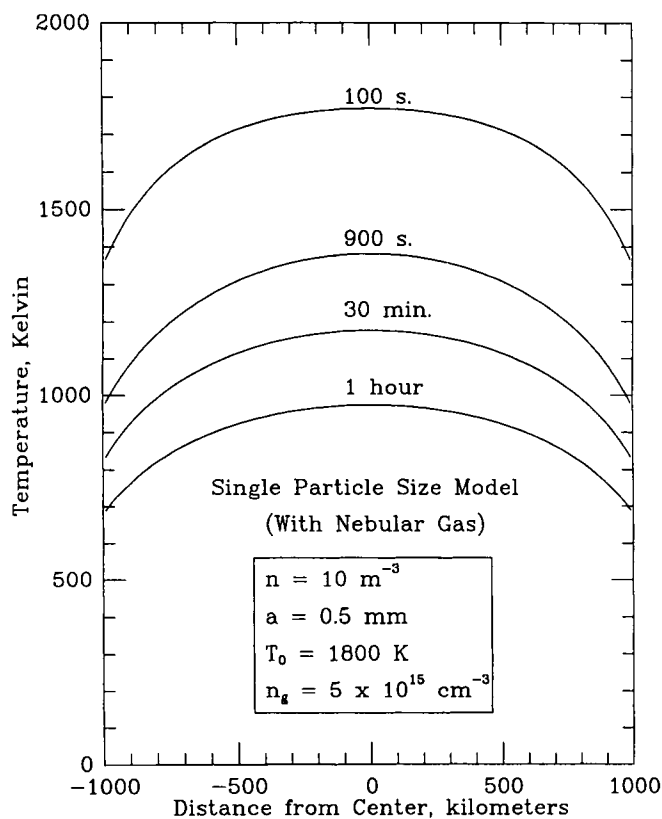


FIG. 6. Same format as Fig. 5 but for a slab containing both 0.5 mm radius particles with number density 10 m^{-3} and a gas with number density $5 \times 10^{15} \text{ cm}^{-3}$ and mean molecular mass $6 \times 10^{-24} \text{ g}$. The slab has a width of 2000 km.

cooling rates for slab widths less than $\sim 600 \text{ km}$ only if a small-scale dust component is added. We therefore consider next a case in which a micron-sized dust component is present in the slab in addition to chondrules and heated gas (cf., "Evidence of Small-Scale Dust Component"). In accordance with the discussion of fine dust optical properties in "Model Formulation", it is necessary to consider emissivities and absorptivities for micron-sized particles ranging from 0.01 to 0.8. In Fig. 8a, an $0.5 \mu\text{m}$ radius dust fraction is added with emissivities and absorptivities of 0.01. As can be seen, a slab width of only 100 km is now sufficient to produce acceptable cooling rates. However, because of the low emission and absorption of these particles, the required dust number density is $1 \times 10^{11} \text{ m}^{-3}$. Assuming a mass density for individual dust particles of 2.5 g cm^{-3} , the corresponding dust mass density in the slab is $1.3 \times 10^{-7} \text{ g cm}^{-3}$, or $\sim 10\times$ the chondrule mass density and $5\times$ the gas mass density. This dust-to-gas mass ratio is 5 to $10\times$ larger than estimated by Liffman and Toscano (2000) from their model for chondrule rim formation. In Fig. 8b, the emissivities and absorptivities of the $0.5 \mu\text{m}$ radius dust fraction are changed to 0.8. In this case, a slab width of 100 km is again possible but with a greatly reduced dust number density of $2 \times 10^9 \text{ m}^{-3}$, representing 20% of the chondrule mass density and 10% of the gas mass density.

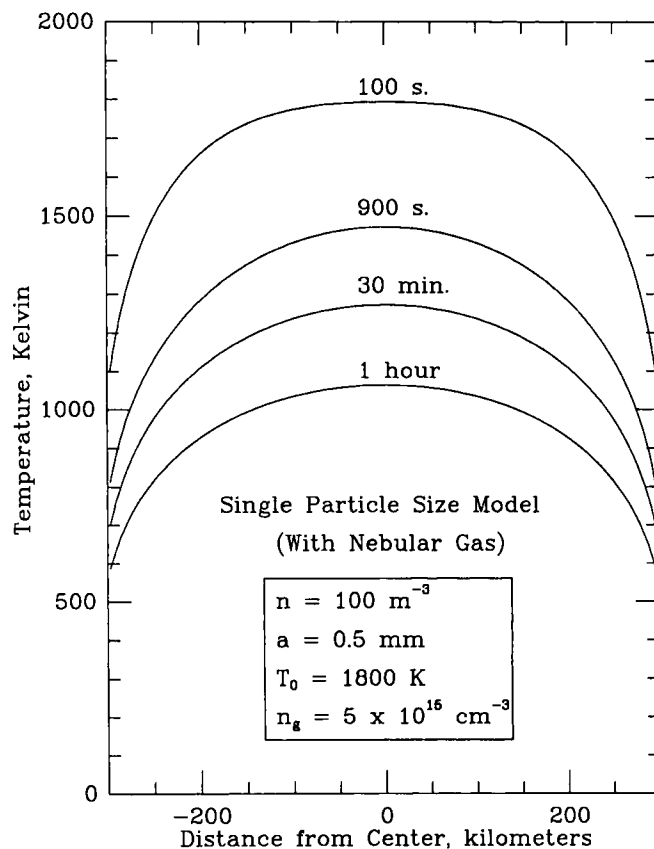


FIG. 7. Same format as Fig. 5 but for a slab containing both 0.5 mm radius particles with number density 100 m^{-3} and a gas with number density $5 \times 10^{16} \text{ cm}^{-3}$. The slab has a width of 600 km.

We note that the simulation of Fig. 8b is approximately consistent with results reported by Sahagian and Hewins (1992). They were able to produce acceptable cooling rates for a chondrule number density of 10 m^{-3} and a slab width of 100 km if a micron-sized dust fraction representing 0.135 of the chondrule mass was added. In our case, the micron-sized fraction is slightly more massive (0.20 of the chondrule mass) and the model includes a relatively minor contribution from the heat capacity of a dense interspersed gas. Since the absorptivities and emissivities adopted for the simulation of Fig. 8b had values of 0.8, the simulations of Sahagian and Hewins also presumably employed values near to unity.

We next investigate whether even smaller scale sizes of chondrule formation regions would yield acceptable cooling rates if larger fine dust densities are assumed. Again, it is necessary to consider a range of dust optical properties (emissivities and absorptivities from 0.8 to 0.01). Figure 9a shows the result of a simulation assuming emissivities and absorptivities of 0.01 for micron-sized dust. For a chondrule number density of 10 m^{-3} and a slab width of 10 km, acceptable cooling rates were obtained if dust number densities of $2 \times 10^{12} \text{ m}^{-3}$ were added. The corresponding dust mass

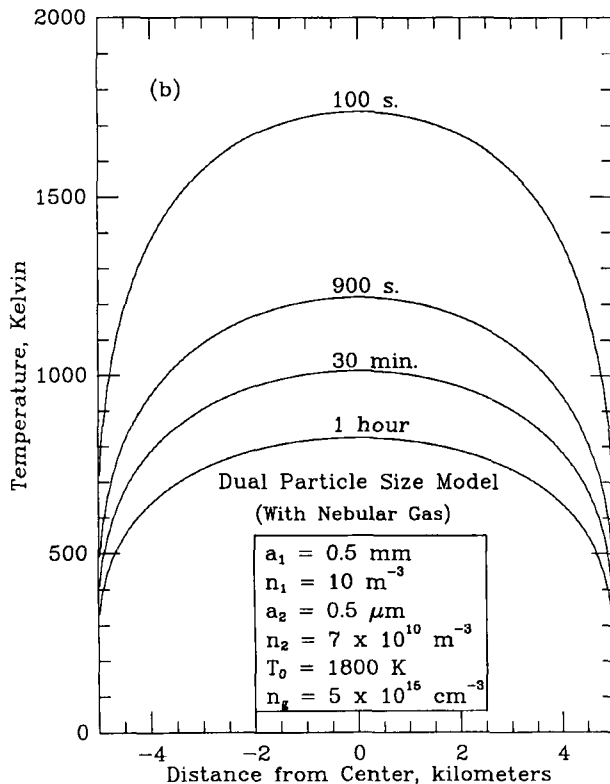
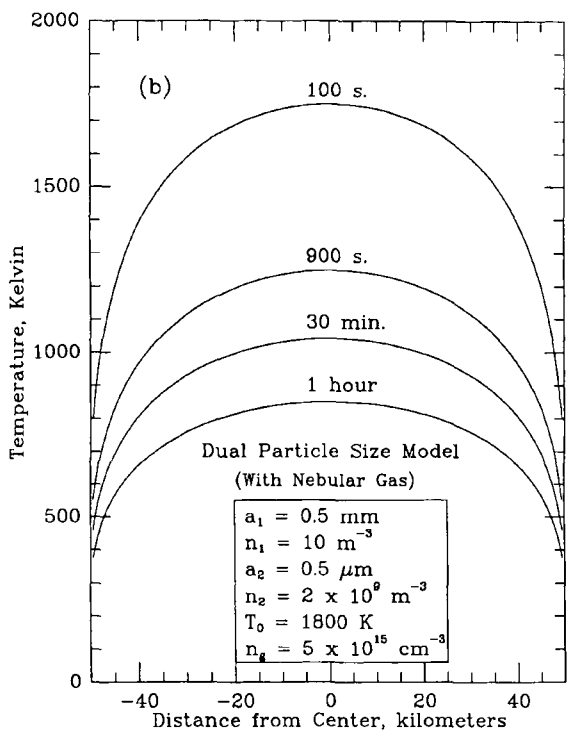
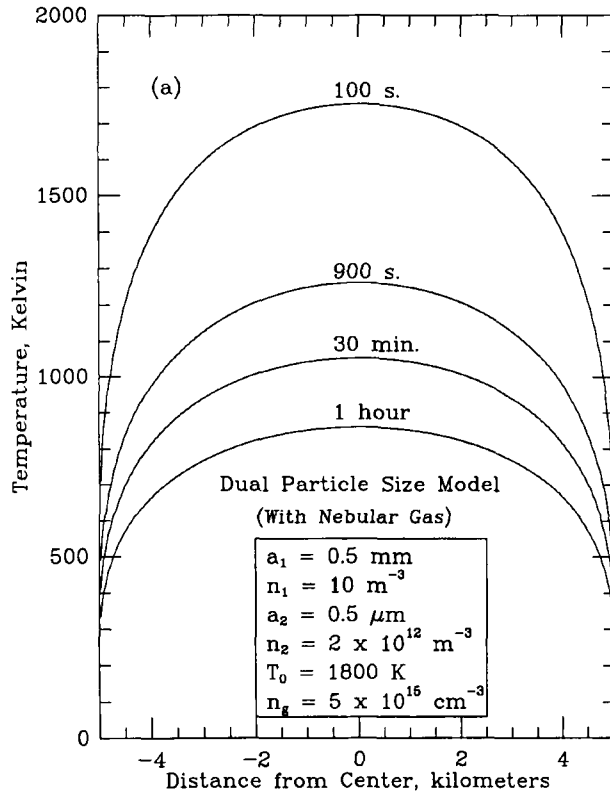
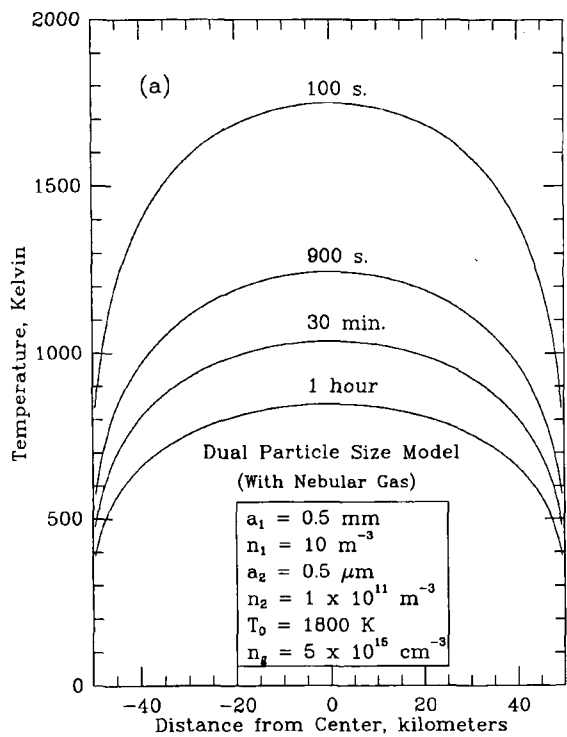


FIG. 8. (a) Same format as Fig. 5 but for a slab containing micron-sized dust in addition to chondrule-sized particles with number density 10 m^{-3} and a gas with number density $5 \times 10^{15} \text{ cm}^{-3}$. The dust emissivity and absorptivity were assumed to have values of 0.01 and the dust number density is $1 \times 10^{11} \text{ m}^{-3}$. The width of the slab is 100 km. (b) Same as part (a) except that the dust emissivity and absorptivity are assumed to have values of 0.8 and the dust number density is decreased to $2 \times 10^9 \text{ m}^{-3}$.

FIG. 9. (a) Temperature profiles for the same calculation as in Fig. 8a except that the dust number density is increased to $2 \times 10^{12} \text{ m}^{-3}$ and the slab width is reduced to 10 km. (b) Same calculation as in Fig. 8b except that the dust number density is increased to $7 \times 10^{10} \text{ m}^{-3}$ and the slab width is reduced to 10 km.

density of $2.6 \times 10^{-6} \text{ g cm}^{-3}$ is a factor of $200\times$ larger than the mass density of the chondrules and is $\sim 100\times$ larger than the mass density of the interspersed gas. Figure 9b shows the result of a simulation assuming emissivities and absorptivities of 0.8 for micron-sized dust. The chondrule number density and slab width are the same as for Fig. 9a. It can be seen that acceptable cooling rates were obtained for fine dust number densities of $7 \times 10^{10} \text{ m}^{-3}$. The corresponding dust mass density is $7\times$ larger than the mass density of the chondrules and $3.5\times$ larger than that of the gas.

It should be noted that dust mass densities may be significantly lower if individual particles consist of loose agglomerations (as expected for accreted condensates, for example). If the mass density of an individual dust particle is only $\sim 1 \text{ g cm}^{-3}$ rather than 2.5 g cm^{-3} , as assumed above, then the dust mass density would be reduced by a corresponding factor. For this reason, actual dust mass densities needed to yield acceptable cooling rates for slab widths as small as 10 km may not be significantly larger than either the chondrule mass density or the gas mass density.

DISCUSSION AND IMPLICATIONS

The results of the previous section show that if radiation from surrounding chondrules, dust, and gas are responsible for inferred chondrule cooling rates, then the scale size of chondrule formation regions can be estimated provided that the concentration and optical properties of fine dust are known. If no dust is present, then rather large-scale sizes for chondrule formation regions (greater than $\sim 1000 \text{ km}$) are required for maximum likely chondrule number densities of $10\text{--}100 \text{ m}^{-3}$ (see Fig. 5). The addition of a heated, dense gas in thermal equilibrium with the chondrules reduces the required scale sizes somewhat but the scale sizes are still greater than $\sim 600 \text{ km}$ (see Figs. 6 and 7).

Adding a fine dust component consisting of micron-sized particles reduces the required scale size significantly. If micron-sized dust emissivities and absorptivities are assumed to be 0.01 (appropriate for perfect Mie spheres with a pure monomineralic composition), then, as shown in Fig. 9a, scale sizes as small as 10 km can be achieved only for dust mass densities at least $25\times$ larger than the gas mass density and $80\times$ that of the chondrules (assuming 10 chondrules per cubic meter and a density for individual dust particles of 1 g cm^{-3}). These dust-to-gas mass ratios are significantly larger than the experimentally inferred estimates of "Solid Particle Densities and Gas Oxygen Fugacities" (≥ 3 to 5). However, if actual micron-sized particles (with irregular shapes and a more complex composition) had emissivities and absorptivities nearer to unity, then, as shown in Fig. 9b, scale sizes as small as 10 km can be achieved for dust mass densities comparable to that of the gas and a few times that of the chondrules (again assuming a mass density within individual dust particles of 1 g cm^{-3}). These dust-to-gas mass ratios are similar to those estimated,

for example, by Liffman and Toscano (2000) from their model for chondrule rim formation. Thus, when all uncertainties are considered, relatively small scale sizes (10–100 km) are possible for chondrule formation regions if micron-sized dust was present with a mass density comparable to that of the chondrules.

It should be noted that for sufficiently large dust concentrations, the chondrules contribute negligibly to the opacity of the system. Thus, for this case, relatively low chondrule number densities of $0.1\text{--}1 \text{ m}^{-3}$ are allowed and our conclusions are not dependent on the assumption of high chondrule number densities as inferred by, for example, Gooding and Keil, (1981); see "Solid Particle Densities and Gas Oxygen Fugacities".

Within the context of the nebular shock wave model for chondrule formation, these results imply that both large-scale shock generation mechanisms (*e.g.*, the gravitational instability mechanism; Wood, 1996; Boss, 2000) and small-scale shock generation mechanisms (*e.g.*, the planetesimal bow shock mechanism; Hood, 1998; Weidenschilling *et al.*, 1998) could, in principle, have produced chondrule cooling rates compatible with meteoritic constraints. Large-scale mechanisms (*e.g.*, the gravitational instability mechanism) have the advantage of yielding sufficiently slow cooling rates for relatively low chondrule number densities without the presence of fine dust (Iida *et al.*, 2001; Desch and Connolly, 2001; Ciesla and Hood, 2001). However, most large-scale mechanisms (gravitational instabilities, proto-solar outbursts) have the disadvantage that they would have been operative primarily during the earliest period of nebula evolution. If chondrule formation persisted for several million years (*e.g.*, Russell *et al.*, 1997), then it is questionable whether these large-scale mechanisms could have continued over such a long time period. Consequently, mechanisms that could have operated over such a time period (*e.g.*, planetesimal bow shocks) may be needed to explain the continued production of chondrules beyond the early massive disk stage of nebular evolution.

The presence of fine dust, as needed to allow small-scale sizes for chondrule formation regions, is indicated by the observation that most unaltered chondrules possess fine-grained rims that can be interpreted as due to hypersonic interaction of freshly formed chondrules with a mixture of gas and dust (Connolly and Love, 1998; Liffman and Toscano, 2000). As noted in "Evidence of Small-Scale Dust Component", a comparison of the second panels of Figs. 2 and 3 indicates that a relative velocity of the order of 1–2 km/s between micron-sized and chondrule-sized particles will result from passage of a gas dynamic shock through a solids-rich zone. This induced relative velocity may have been sufficient to produce dust mantles by collisions with freshly formed chondrules. After the chondrule-dust relative velocity had decreased to nearly zero, the cooling rate of the chondrules would have been strongly influenced by the dust density, as shown in "Model Results". Although much (nearly half) of the micron-sized particle was vaporized in the simulation of Fig. 3, the adopted

emissivity (2×10^{-3}) may have been unrealistically low. Even if micron-sized dust was partially vaporized during shock passage, recondensation would have increased the dust density again downstream from the shock front. Survival or regeneration of micron-sized dust is of course necessary if such dust contributed to chondrule rim formation.

While the emphasis of the simulations reported here was on cooling rates, it is important to note that larger chondrule and/or dust densities may also have acted to buffer the range of chondrule maximum temperatures reached during the passage of nebular shocks. Single chondrule precursors encountering nebular shocks would be partially or completely melted only for a narrow range of sonic Mach numbers. Larger Mach numbers would vaporize the precursor while smaller Mach numbers would fail to melt the precursor. Mutual radiation from surrounding chondrules tends to equilibrate temperatures in a dense zone with high number densities (e.g., Hood and Horanyi, 1991, 1993). Partial vaporization of chondrule components with lower vaporization temperatures would also have released a dense silicate vapor in the near vicinity of the chondrule. This temporary chondrule "atmosphere" would have tended to reduce the rate of drag heating, thereby preventing further temperature increases.

To date, as in the present paper, only limited portions of the full coupled problem of chondrule formation by shock processing in a solids-rich gas have been solved. Hood and Horanyi (1993) considered the time-dependent problem of the interaction of a one-dimensional solid particle cloud with a radiative gas dynamic shock. They found that larger solids number densities resulted in more rapid melting of precursor particles near the upstream edge of the solid particle cloud owing to increased radiative heating by surrounding dust. Because of limitations of the numerical code, calculations could not be carried forward far enough in time to estimate cooling rates. Iida *et al.* (2001) have recently presented a much more detailed simulation of the single-particle shock model that explicitly includes chemical reactions and radiative cooling of the shock-heated nebula gas by atomic and molecular emissions. They found that melting without complete vaporization of precursor millimeter-sized silicate particles would occur only for shock velocities (Mach numbers, M) within a narrow range of 6 to 7 km/s ($M \approx 4$ to 5) for an initial nebula number density of 10^{15} cm $^{-3}$. Ciesla and Hood (2001, unpubl. data) have considered the steady state problem of the passage of a radiative shock wave through a solids-gas suspension in the nebula. Again, melting without vaporization of precursor particles was possible only for a narrow range of Mach numbers. The latter numerical simulations explicitly accounted for gas-solids energy and momentum transfer across the shock (Igra and Ben-Dor, 1980). Cooling rates were determined by radiation from chondrules balanced by thermal collisional energy transfer from the shock-heated gas to the chondrules. However, these calculations did not consider partial vaporization of chondrule precursors or the possible presence of micron-sized dust in the

solids-rich zone. Downstream cooling of the shocked gas resulting from gas chemistry, dissociation, and recondensation were also neglected. Finally, Desch and Connolly (2001) have recently reported a new shock model simulation which includes hydrogen dissociation, recombination, and radiative heating by surrounding dust. It was found that radiation from hot chondrules near the shock front can represent a significant persistent energy source for melted precursors as they travel downstream, thereby reducing cooling rates to an acceptable level. However, the reduced cooling rates were found only for a solar solids-to-gas mass ratio (0.005) which allowed the receding chondrules to receive direct radiation from heated gas and solids near the shock front.

Work toward a complete solution of the multiple-particle shock problem is currently underway by several research groups. A full solution will provide further insight into whether and how the shock model can be consistent with the derived thermal conditions of chondrule formation.

Acknowledgments—This work was supported by a grant from NASA's Origins program. We thank David Kring for useful discussions and advice relating to the interpretation of meteoritic data. Stan Love, an anonymous reviewer, and the associate editor, Pat Cassen, provided detailed comments and criticisms of an earlier manuscript that resulted in significant improvements to the paper. Helpful discussions with Bashar Rizk and Denton Ebel are also gratefully acknowledged.

Editorial handling: P. Cassen

REFERENCES

- ALEXANDER C. M. O'D. (1994) Chondrules from chondrules? An ion probe trace element study (abstract). *Lunar Planet. Sci.* **25**, 7–8.
- BARROW G. (1966) *Physical Chemistry*. McGraw Hill, New York, New York, USA. 843 pp.
- BECKETT J. R. AND STOLPER E. (2001) Constraints on the evolution of chondrules based on the moderately volatile elements sulfur, sodium, and potassium (abstract). *Lunar Planet. Sci.* **32**, #1730, Lunar and Planetary Institute, Houston, Texas, USA (CD-ROM).
- BOSS A. P. (1996) A concise guide to chondrule formation models. In *Chondrules and the Protoplanetary Disk* (eds. R. H. Hewins, R. H. Jones and E. R. D. Scott), pp. 257–264. Cambridge University Press, New York, New York, USA.
- BOSS A. P. (2000) Possible rapid gas giant planet formation in the solar nebula and other protoplanetary disks. *Astrophys. J.* **536**, L101–L104.
- CASSEN P. (1996) Models for the fractionation of moderately volatile elements in the solar nebula. *Meteorit. Planet. Sci.* **31**, 793–806.
- CONNOLLY H. AND LOVE S. (1998) The formation of chondrules: Petrologic tests of the shock wave model. *Science* **280**, 62–67.
- CUZZI J. N., DOBROVLSKIS A. R. AND HOGAN R. C. (1996) Turbulence, chondrules, and planetesimals. In *Chondrules and the Protoplanetary Disk* (eds. R. H. Hewins, R. H. Jones and E. R. D. Scott), pp. 35–44. Cambridge University Press, New York, New York, USA.
- CUZZI J. N., HOGAN R. C., PAQUE J. M. AND DOBROVLSKIS A. R. (2001) Size-selective concentration of chondrules and other small particles in protoplanetary nebula turbulence. *Astrophys. J.* **546**, 496–508.
- DESCH S. AND CONNOLLY H. (2001) Melting of chondrules and type B CAIs by nebular shocks (abstract). *Lunar Planet. Sci.*

- 32, #2163, Lunar and Planetary Institute, Houston, Texas, USA (CD-ROM).
- DESCH S. AND CUZZI J. (2000) The generation of lightning in the solar nebula. *Icarus* **143**, 87–105.
- EBEL D. S. AND GROSSMAN L. (2000) Condensation in dust-enriched systems. *Geochim. Cosmochim. Acta* **64**, 339–366.
- GALY A., YOUNG E. D., ASH R. D. AND O'NIONS R. K. (2000) The formation of chondrules at high gas pressures in the solar nebula. *Science* **290**, 1751–1753.
- GOODING J. L. AND KEIL K. (1981) Relative abundances of chondrule primary textural types in ordinary chondrites and their bearing on conditions of chondrule formation. *Meteoritics* **16**, 17–43.
- GROSSMAN J. N. (1988) Formation of chondrules. In *Meteorites and the Early Solar System* (eds. J. F. Kerridge and M. S. Matthews), pp. 680–696. Univ. Arizona Press, Tucson, Arizona, USA.
- GROSSMAN J. N. (1996) Chemical fractionations of chondrites: Signatures of events before chondrule formation. In *Chondrules and the Protoplanetary Disk* (eds. R. H. Hewins, R. H. Jones, and E. R. D. Scott), pp. 243–256. Cambridge Univ. Press, New York, New York, USA.
- GROSSMAN J. N., RUBIN A. E., NAGAHARA H. AND KING E. A. (1988) Properties of chondrules. In *Meteorites and the Early Solar System* (eds. J. F. Kerridge and M. S. Matthews), pp. 680–696. Univ. Arizona Press, Tucson, Arizona, USA.
- HEWINS R. (1988) Experimental studies of chondrules. In *Meteorites and the Early Solar System* (eds. J. Kerridge and M. Matthews), pp. 660–679. Univ. Arizona Press, Tucson, Arizona, USA.
- HEWINS R. (1997) Chondrules. *Ann. Rev. Earth Planet. Sci.* **25**, 61–84.
- HEWINS R. H. AND RADOMSKY P. M. (1990) Temperature conditions for chondrule formation. *Meteoritics* **26**, 309–318.
- HOOD L. L. (1998) Thermal processing of chondrule precursors in planetesimal bow shocks. *Meteorit. Planet. Sci.* **33**, 97–107.
- HOOD L. L. AND HORANYI M. (1991) Gas dynamic heating of chondrule precursor grains in the solar nebula. *Icarus* **93**, 259–269.
- HOOD L. L. AND HORANYI M. (1993) The nebular shock wave model for chondrule formation: One-dimensional calculations. *Icarus* **106**, 179–189.
- IGRA O. AND BEN-DOR G. (1980) Parameters affecting the relaxation zone behind normal shock waves in a dusty gas. *Isr. J. Tech.* **18**, 159–168.
- IIDA A., NAKAMOTO T., SUSA H. AND NAKAGAWA Y. (2001) A shock heating model for chondrule formation in a protoplanetary disk. *Icarus*, (in press).
- KRING D. A. (1988) The petrology of meteoritic chondrules: Evidence for fluctuating conditions in the solar nebula. Ph.D. Thesis, Harvard Univ., Cambridge, Massachusetts, USA.
- KRING D. A. (1991) High temperature rims around chondrules in primitive chondrites: Evidence for fluctuating conditions in the solar nebula. *Earth Planet. Sci. Lett.* **105**, 65–80.
- KROT A., MEIBOM A., RUSSELL S., ALEXANDER C. M. O'D., JEFFRIES T. AND KEIL K. (2001) A new astrophysical setting for chondrule formation. *Science* **291**, 1776–1779.
- LAURETTA D. S., BUSECK P. R. AND ZEGA T. J. (2001) Opaque minerals in the matrix of the Bishunpur (LL3.1) chondrite: Constraints on the chondrule formation environment. *Geochim. Cosmochim. Acta* **65**, 1337–1353.
- LIFFMAN K. AND TOSCANO M. (2000) Chondrule fine-grained mantle formation by hypervelocity impact of chondrules with a dusty gas. *Icarus* **143**, 106–125.
- LUGMAIR G. W. AND SHUKOLYUKOV A. (2001) Early solar system events and timescales. *Meteorit. Planet. Sci.* **36**, 1017–1026.
- MACPHERSON G. J., WARK D. A. AND ARMSTRONG J. T. (1988) Primitive material surviving in chondrites: Refractory inclusions. In *Meteorites and the Early Solar System* (eds. J. F. Kerridge and M. Matthews), pp. 746–807. Univ. Arizona Press, Tucson, Arizona, USA.
- METZLER K. AND BISCHOFF A. (1996) Constraints on chondrite agglomeration from fine-grained chondrule rims. In *Chondrules and the Protoplanetary Disk* (eds. R. H. Hewins, R. H. Jones and E. R. D. Scott), pp. 153–161. Cambridge Univ. Press, New York, New York, USA.
- METZLER K., BISCHOFF A. AND STÖFFLER D. (1992) Accretionary dust mantles in CM chondrites: Evidence for solar nebula processes. *Geochim. Cosmochim. Acta* **56**, 2873–2897.
- RADOMSKY P. M. AND HEWINS R. H. (1990) Formation conditions of pyroxene-olivine and magnesian-olivine chondrules. *Geochim. Cosmochim. Acta* **54**, 3475–3490.
- RIZK B., HUNTEN D. M. AND ENGEL S. (1991) Effects of size-dependent emissivity on maximum temperatures during micrometeorite entry. *J. Geophys. Res.* **96**, 1303–1314.
- RUSSELL S. S., HUSS G. R., MACPHERSON G. J. AND WASSERBURG G. J. (1997) Early and late chondrule formation: New constraints for solar nebula chronology from $^{26}\text{Al}/^{27}\text{Al}$ in unequilibrated ordinary chondrites (abstract). *Lunar Planet. Sci.* **28**, 1209–1210.
- SAHAGIAN D. L. AND HEWINS R. H. (1992) The size of chondrule-forming events (abstract). *Lunar Planet. Sci.* **23**, 1197–1198.
- SEARS D. G., HUANG S. AND BENOIT P. H. (1996) Open-system behavior during chondrule formation. In *Chondrules and the Protoplanetary Disk* (eds. R. H. Hewins, R. H. Jones, and E. R. D. Scott), pp. 221–231. Cambridge University Press, New York, New York, USA.
- SHU F. H., SHANG H., GOUNELLE M., GLASSGOLD A. E. AND LEE T. (2001) The origin of chondrules and refractory inclusions in chondritic meteorites. *Astrophys. J.* **548**, 1029–1050.
- TAYLOR G. J., SCOTT E. R. D. AND KEIL K. (1983) Cosmic setting for chondrule formation. In *Chondrules and Their Origins* (ed. E. A. King), pp. 262–278. Lunar and Planetary Institute, Houston, Texas, USA.
- WEIDENSCHILLING S. J. (1988) Formation processes and time scales for meteorite parent bodies. In *Meteorites and the Early Solar System* (eds. J. F. Kerridge and M. S. Matthews), pp. 680–696. Univ. Arizona Press, Tucson, Arizona, USA.
- WEIDENSCHILLING S. J., MARZARI F. AND HOOD L. L. (1998) The origin of chondrules at Jovian resonances. *Science* **279**, 681–684.
- WOOD J. A. (1984) On the formation of meteoritic chondrules by aerodynamic drag heating in the solar nebula. *Earth Planet. Sci. Lett.* **70**, 11–26.
- WOOD J. A. (1985) Meteoritic constraints on processes in the solar nebula. In *Protostars and Planets II* (eds. D. C. Black and M. S. Matthews), pp. 687–702. Univ. Arizona Press, Tucson, Arizona, USA.
- WOOD J. A. (1996) Processing of chondritic and planetary materials in shocks associated with spiral density waves in the solar nebula (abstract). *Lunar Planet. Sci.* **27**, 1453–1454.
- WOOD J. A. AND HASHIMOTO A. (1993) Mineral equilibrium in fractionated nebular systems. *Geochim. Cosmochim. Acta* **57**, 2377–2388.

APPENDIX

The appendix appears on the following pages.

APPENDIX A

An estimate for the ambient midplane nebular gas density in the asteroid belt region (~ 2.5 AU) corresponding to a total disk mass of 10% of the solar mass (near the upper limit for a "minimum-mass" nebula) can be obtained as follows.

In general (see, for example, Hood, 1998), the column mass density of a nebula in approximate hydrostatic equilibrium perpendicular to the midplane at radial distance r is given by

$$\sigma_m(r) = \pi^{1/2} H \bar{m} n(r, 0) \quad (\text{A1})$$

where H is the scale height, \bar{m} is the mean molecular mass, $n(r, 0)$ is the gas number density at distance r and height above the midplane $z=0$. For a nebula with a Gaussian midplane number density distribution (e.g., Cassen, 1996), we have

$$n(r, 0) \cong n(r_0, 0) \exp(-(r-r_0)^2 / r_0^2) \quad (\text{A2})$$

where r_0 is some reference radius much less than the extent of the disk (usually taken as 1 AU). For this case, the total disk mass is

$$M_d = \int_0^\infty \sigma_m(r) 2\pi r dr \cong \pi r_0^2 \sigma_m(r_0) \exp(-1) \quad (\text{A3})$$

For the case in which the temperature is approximately independent of the vertical coordinate in the disk, the scale height is $H^2 = 2k\bar{T}^3/GM_\star\bar{m}$, where k is Boltzmann's constant, \bar{T} is the mean temperature at radius r , G is the gravitational constant, and M_\star is the mass of the protosun. Taking $\bar{T} \approx 632$ K at $r_0 = 1$ AU, we obtain $H(r_0) \approx 1.05 \times 10^{12}$ cm. Inserting this value into Eqs. (A1) and (A3), one finds that total disk masses of $0.1 M_\star$ are possible provided that $n(r_0) \approx 1 \times 10^{17}$ cm $^{-3}$. From Eq. (A2), it follows that $n(2.5$ AU) is $\sim 2 \times 10^{14}$ cm $^{-3}$.

APPENDIX B

We consider a case in which the slab of Fig. 4 contains more than one particle component, each consisting of identical spheres with some specified diameter. In this derivation, the possible presence of nebular gas is neglected. Each particle component is characterized by a geometrical cross section of $\sigma_p^{(m)}$, an emissivity of $\epsilon_{\text{em}}^{(m)}$, a number density of $n_p^{(m)}$, a temperature of $T^{(m)}$, and an absorptivity of $\epsilon^{(m)}$, where the superscript m denotes the particle component. For example, in a two-component particle model, $m = 1$ would denote the larger particle component and $m = 2$ would denote the smaller component. For a slab containing a total of q particle components, the energy flux in the positive x direction out of the i th layer (equivalent to Eq. (3)) is

$$f_p(i) = \sum_{m=1}^q f_p^{(m)} \quad (\text{B1})$$

where

$$f_p^{(m)} = \epsilon_{\text{em}}^{(m)} n_p^{(m)} \sigma_p^{(m)} T^{(m)4}(i) \quad (\text{B2})$$

The energy flux in the negative x direction out of the same layer is

$$f_n(i) = \sum_{m=1}^q f_n^{(m)}(i) \quad (\text{B3})$$

where $f_n^{(m)}(i) = -f_p^{(m)}$. At the j th boundary between layers, the energy flux across the boundary due to radiation from the i th layer is

$$F(i, j) = f_p(i) \times (1 - \sum_{m=1}^q \epsilon_{\text{abs}}^{(m)} n_p^{(m)} \sigma_p^{(m)} dx)^n \quad (\text{B4})$$

for $j > i$, where $n = |j - i - 1|$. For $j \leq i$,

$$F(i, j) = f_n(i) \times (1 - \sum_{m=1}^q \epsilon_{\text{abs}}^{(m)} n_p^{(m)} \sigma_p^{(m)} dx)^n \quad (\text{B5})$$

where $n = |j - i|$. The total positively directed and negatively directed fluxes at the j th boundary are again given by Eq. (6) and (7), respectively. At $t = 0$, the total thermal energy per unit area in the i th layer is

$$E_i = \sum_{m=1}^q E_i^{(m)} \quad (\text{B6})$$

where $E_i^{(m)} = n_p^{(m)} m_p^{(m)} C_p T^{(m)} dx$. After a time increment dt , the m th particle component gains an increment of energy given by

$$dE_g^{(m)}(i) = (F_p(j) + |F_n(j+1)|) dt \times (\epsilon_{\text{abs}}^{(m)} n_p^{(m)} \sigma_p^{(m)} dx) \quad (\text{B7})$$

The m th particle component in the same layer loses a thermal energy increment given by

$$dE_l^{(m)}(i) = (f_p^{(m)}(i) + |f_n^{(m)}(i)|) dt \quad (\text{B8})$$

At each time step, the total energy of each particle component in the i th layer is adjusted according to

$$E_i^{(m)}(t + dt) = E_i^{(m)}(t) + dE_g^{(m)}(i) - dE_l^{(m)}(i)$$

The temperature of each particle component at time $t + dt$ is then given by

$$T_i^{(m)}(t + dt) = E_i^{(m)}(t + dt) / (n_p^{(m)} m_p^{(m)} C_p dx) \quad (\text{B9})$$

APPENDIX C

In this appendix, we wish to calculate the net flux of radiation from a layer of thickness dx containing spherical particles of radius a , temperature T , and emissivity ϵ_{em} . For simplicity, we first consider a case in which there is no attenuation of the radiation outside the layer.

We use cylindrical coordinates r, ϕ, x , where x is the axis perpendicular to the layer, r is radial distance from the origin in the plane of the layer, and ϕ is azimuthal angle in the layer. In order to calculate the flux at $r = 0$ and at some distance x above the layer, consider an arbitrary cylindrical volume element $rdrd\phi dx$ located at $r, \phi, 0$. The flux emitted from the surface of this volume element toward the observation point at $0, \phi, x$ is reduced by a factor of $\cos\theta = x/(x^2 + r^2)^{1/2}$. Also, the component of the flux from that volume element in the \hat{x} direction at $0, \phi, x$ is reduced by the same factor of $\cos\theta$. By symmetry, one may therefore write the contribution to the total flux at $0, \phi, x$ due to radiation from the azimuthally integrated volume element $2\pi r dr dx$ as

$$dJ(0, x) = n_p (2\pi r dr) dx (4\pi a^2 \epsilon_{em} \sigma T^4) \times \frac{1}{4\pi(r^2 + x^2)} \times \frac{x}{(r^2 + x^2)^{1/2}} \times \frac{x}{(r^2 + x^2)^{1/2}} \quad (C1)$$

Integrating over radial distance in the layer from $r = 0$ to ∞ , the net flux perpendicular to the layer is

$$J(0, x) = n_p (2\pi a^2 \epsilon_{em} \sigma T^4) x^2 dx \int_0^\infty \frac{r dr}{(r^2 + x^2)^2} \quad (C2)$$

or

$$J(0, x) = n_p (\pi a^2 \epsilon_{em} \sigma T^4) dx \quad (C3)$$

For a layer of infinite extent with no attenuation outside of the layer, therefore, the flux is independent of the value of x .

Now consider a case in which the flux from the layer is attenuated by intervening spherical particles. The intervening particles are also assumed to be of radius a and the observation point is located at $r = 0$ and $x = \delta x$. Radiation from an arbitrary volume element $rdrd\phi dx$ located at $r, \phi, 0$ will be attenuated at the observation point by a factor of $\exp(-\alpha(r^2 + \delta x^2)^{1/2})$, where $\alpha = \epsilon_{abs} n_p \pi a^2$. The net flux perpendicular to the layer at $0, \phi, \delta x$ is therefore given by

$$J(0, \delta x) = n_p (2\pi a^2 \epsilon_{em} \sigma T^4) \delta x^2 dx \int_0^\infty \frac{r dr}{(r^2 + \delta x^2)^2} \times \exp(-\alpha(r^2 + \delta x^2)^{1/2}) \quad (C4)$$

Evaluating the integral yields

$$J(0, \delta x) = n_p (2\pi a^2 \epsilon_{em} \sigma T^4) \delta x^2 dx \times \left(\frac{\exp(-\alpha \delta x)}{\delta x^2} - \alpha^2 \exp(-\alpha \delta x) \int_0^\infty \frac{\exp(-t) dt}{(\alpha x + t)^2} \right) \quad (C5)$$

where t is a "dummy" variable of integration. Finally, we consider a limit in which the intervening layer of absorbing particles is sufficiently thin (δx is sufficiently small) so that the condition $\alpha \delta x \ll 1$ is satisfied. In that case, the exponentials in (C5) may be expanded in a power series and, to lowest order in $\alpha \delta x$, one obtains

$$J(0, \delta x) = n_p (\pi a^2 \epsilon_{em} \sigma T^4) dx (1 - \epsilon_{abs} n_p \pi a^2 \delta x) \quad (C6)$$

If δx is chosen to be equal to dx , then this result shows that the energy flux across a layer boundary in the slab model of "Model Formulation" is attenuated due to absorption in an adjacent layer by the approximate factor $(1 - \epsilon_{abs} n_p \pi a^2 dx)$.